
[Original Paper]
*Journal of the Korean Society
for Nondestructive Testing*
Vol. 31, No. 1 (2011. 2)

Measurements of Sub- and Super Harmonic Waves at the Interfaces of Fatigue-Cracked CT Specimen

Hyunjo Jeong*[†] and Dan Barnard**

Abstract Nonlinear harmonic waves generated at cracked interfaces are investigated both experimentally and theoretically. A compact tension specimen is fabricated and the amplitude of transmitted wave is analyzed as a function of position along the fatigued crack surface. In order to measure as many nonlinear harmonic components as possible a broadband Lithium Niobate (LiNbO₃) transducers are employed together with a calibration technique for making absolute amplitude measurements with fluid-coupled receiving transducers. Cracked interfaces are shown to generate high acoustic nonlinearities which are manifested as harmonics in the power spectrum of the received signal. The first subharmonic ($f/2$) and the second harmonic ($2f$) waves are found to be dominant nonlinear components for an incident toneburst signal of frequency f . To explain the observed nonlinear behavior a partially closed crack is modeled by planar half interfaces that can account for crack parameters such as crack opening displacement and crack surface conditions. The simulation results show reasonable agreements with the experimental results.

Keywords: Acoustic Nonlinearity, Cracked Interface, Subharmonics, Higher Harmonics, Receiver Calibration, Nonlinear Interface Model

1. Introduction

One of the major roles of ultrasonic nondestructive inspection(NDI) is to detect and characterize crack-like flaws in critical components and structures. Both linear and nonlinear ultrasonic techniques can be applied for these purposes. When cracks are open, linear methods based on the time-of-flight-diffraction (TOFD) or a pulse-echo reflection can be a useful tool. However, when cracks are closed or partially closed, it will be more challenging to detect them because the diffracted or reflected signal is too weak. An alternative technique to overcome this limitation is nonlinear ultrasonics. Ultrasonic nonlinearity is manifested as

harmonics (sub or higher) in the power spectrum of the received signal when intense ultrasonic wave is incident into imperfect interfaces. This effect is known as contact acoustic nonlinearity(CAN), and it has been the topic of many research works concerning the characterization of closed cracks or imperfect bond interfaces [1]. Earlier theoretical investigations [2-4] predicted that a weak or incompletely bonded interface will generate high second harmonics when subjected to sufficiently intense acoustic energy, and previous experiments have indicated that acoustic harmonic generation occur on various types of interfaces such as unbounded interfaces [5], microstructural changes [6-9], cracks [10,11],

and adhesive joints [12,13].

Subharmonics are known to be generated only at the crack interface [14-16]. Subharmonics is a nonlinear wave distortion where the amplitude of adjacent carriers becomes different, resulting in the period doubling and frequency of $f/2$ [16-18]. Because the higher harmonics are also generated by the piezoelectric transducers and by the electronic equipment, extraction of subharmonic response could be more reliable indicators of the crack damage. Yamanaka et al. [14] investigated the detailed feature of subharmonics generated at the closed cracks and applied the concept of subharmonic resonance for crack imaging.

Previous experimental studies considered higher harmonics or subharmonics individually for the analysis of cracked interface. Either one of them were frequently ignored. The reason for not being able to extract both harmonic components together in one measurement can be attributed to bandwidth limit of receiving transducers. The present study is concerned with simultaneous measurements of nonlinear harmonic components at cracked interfaces in absolute manner. For this purpose, we fabricated broadband Lithium Niobate (LiNbO_3) transducers. The LiNbO_3 transducers employed in this work has a center frequency of 15 MHz and -6 dB bandwidth of 60%. We also developed a calibration technique for making absolute amplitude measurements with fluid-coupled receiving transducers [19].

This paper is outlined as follows. First, a calibration technique for absolute amplitude measurements is provided. Then, experimental details for extracting both subharmonic and higher harmonic components from a cracked compact tension(CT) specimen are described. Finally, we present simulation results based on the existing interface model to explain the observed nonlinear behavior.

2. Harmonic Generation Experiment

Fig. 1 is a schematic representation of the calibration measurement that is performed prior to the harmonic generation measurement. The purpose of the calibration measurement is to obtain the output signal in terms of the absolute displacement amplitude in the harmonic generation experiment. We use the concept of transfer function $H(\omega)$ that converts the electric output (current) $I_{out}(\omega)$ to the absolute displacement amplitude $A_{inc}(\omega)$ at the reception side of a contact ultrasonic measurement through the following relationship:

$$A_{inc}(\omega) = H(\omega)I_{out}(\omega) \quad (1)$$

This transfer function can be obtained during the calibration phase using a broadband pulse-echo technique. The broadband calibration pulse is produced by a commercial pulser (Panametrics 5052 PR pulser/receiver). This broadband technique establishes an empirical conversion efficiency for the receiving transducer as a function of frequency, allowing the direct calculation of the displacement amplitudes. The calibration procedure consists of measuring the voltage, $V'_{in}(\omega)$, and the current, $I'_{in}(\omega)$, applied to the receiving transducer by a broadband pulser and the output voltage, $V'_{out}(\omega)$, and current, $I'_{out}(\omega)$, from the same transducer after the input pulse has made one round trip through the sample. Assuming the reciprocity of transducer/couplant arrangement and linearity of the measurement system, the transfer function is obtained as (Dace et al., 1992)

$$H(\omega) = \sqrt{\frac{|I'_{in}(\omega) \left(\frac{V'_{out}(\omega)}{I'_{out}(\omega)} \right) + V'_{in}(\omega)|}{2\omega^2 \rho v a |I'_{out}(\omega)|}} \quad (2)$$

where ω is the circular frequency, ρ is the density, v is the longitudinal velocity, and a is the area of the transducer. Here the prime is used to denote a parameter measured during the calibration. Note that the transmitting transducer must not be coupled to the sample during the calibration stage, as a free surface reflection is required to maintain reciprocity. A diffraction correction is applied to the calibration measurement for $H(\omega)$ when the round trip distance through a sample is greater than the distance to the nearfield/farfield transition.

Once the calibration measurements are made, the transmitting transducer is coupled to the sample for the transmission measurement. A monochromatic toneburst at the fundamental frequency is injected into the sample, propagates along the length of the sample and is received by the receiving transducer. The absolute displacement amplitude of the transmitted wave incident on the receiving transducer is calculated from the output current, $I_{out}(\omega)$, using eqn. (1). Fig. 2 shows an equipment block diagram of the harmonic generation measurement system. A function generator (Marconi 2022D) tuned to the fundamental frequency (10 MHz for these measurements) supplies the continuous wave for a gated amplifier (Matec 5100/515A) to provide the high power monochromatic toneburst for the harmonic generation. The two transducers are made of LiNbO_3 wafers (longitudinal polarization) and coupled to the sample with a light oil. The size of the transducer is 12.7 mm in diameter. The transmitter has a center frequency of 10 MHz, while the receiver has a broad bandwidth with a center frequency of 15 MHz. The two transducers are aligned with each other by being placed in a test fixture that can provide a constant pressure during the entire measurement.

The harmonic generation measurements have been made at eight different input fundamental amplitude by using a stepped attenuator (0, 1, 2,

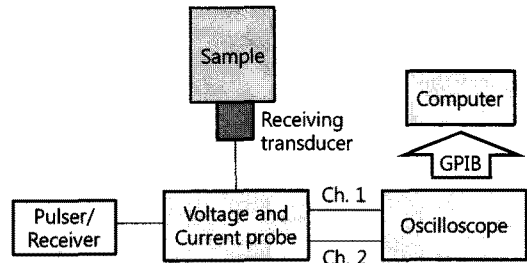


Fig. 1 Schematic diagram for calibration of receiving transducer

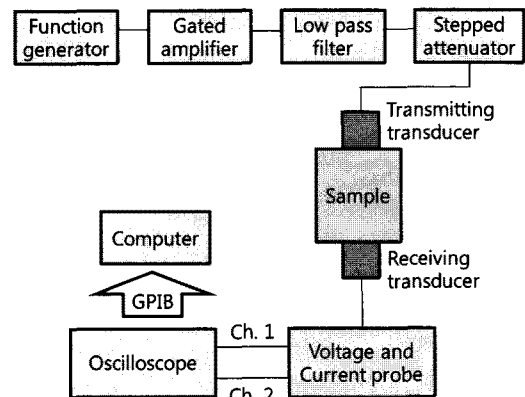


Fig. 2 Schematic diagram for harmonic generation measurement

3, 4, 5, 6, 10 dB) in the circuit between the gated amplifier output and the transmitting transducer. The nonlinearity parameter for the first subharmonic component ($\beta'_{1/2} = A_{1/2}/A_1^2$) is obtained from the slope of the $A_{1/2}$ versus A_1^2 plot. Similarly, the nonlinearity parameter for the second harmonic component ($\beta'_2 = A_2/A_1^2$) is obtained from the slope of the A_2 versus A_1^2 plot. Here, A_1 , $A_{1/2}$ and A_2 represent the magnitude of Fourier spectrum of the received wave at the fundamental ($f=10$ MHz), the first subharmonic ($f/2=5$ MHz), and the second harmonic frequency ($2f=20$ MHz), respectively.

A compact tension (CT) specimen of Al 6061-T6 is used in this work. This cracked specimen was fabricated by applying a high cycle fatigue loading on a chevron notch. Fig. 3 shows the schematic configuration of the

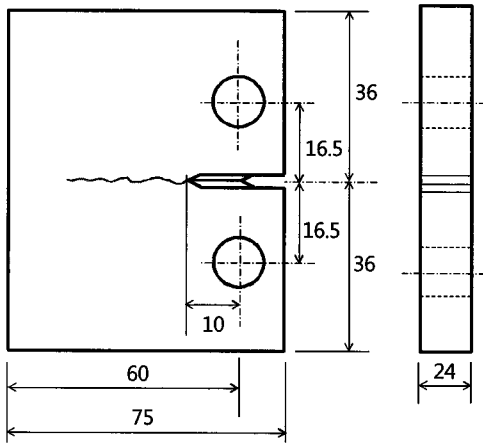


Fig. 3 Configuration of CT specimen with fatigue crack (unit: mm)

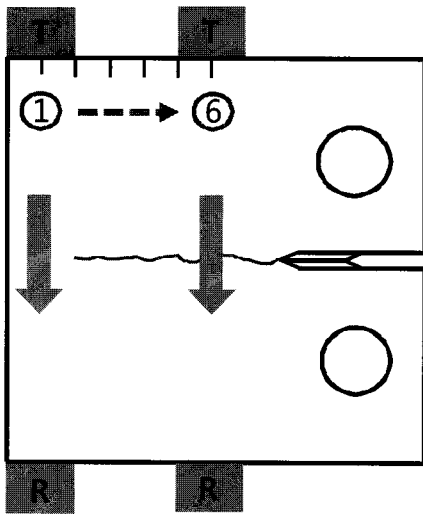


Fig. 4 Harmonic generation measurements at six positions along the cracked interface

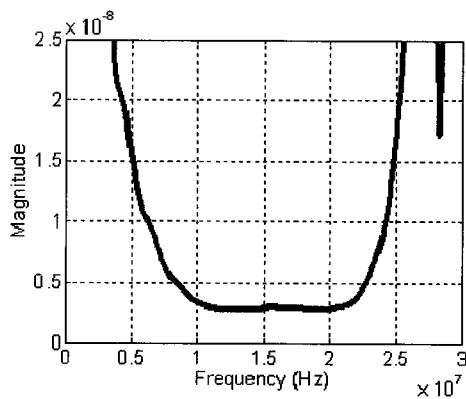


Fig. 5 Example of a typical transfer function

cracked CT specimen. The crack length was measured to be about 40 mm from the notch center.

Harmonic generation measurements are made in the through transmission mode at six different positions along the cracked interface as shown in Fig. 4. The measurement interval in this case is 5 mm.

3. Results and Discussion

Fig. 5 shows a typical transfer function obtained with the calibration measurement system. This function is acquired from the measurement at the position 1 on the cracked CT specimen (Fig. 4) and used for the calibration purpose in harmonic generation measurements at all six positions. It is noted that the receiving transducer seems to have a broad bandwidth in the region of interest (5-25 MHz).

The received signals before and after calibration are shown in Fig. 6 together with corresponding Fourier spectra. This signal is obtained from the measurement position 2. The input signal used is the monochromatic toneburst of the centerfrequency $f=10$ MHz, and amplified with a gated amplifier up to 150 V_{p-p}. This value corresponds to the 0 dB amplification out of eight different input levels used. The received signal is then calibrated using the transfer function. After calibration, the absolute displacement of the output signal turned out to be about 60 nm peak-to-peak as shown in Fig. 6(b). In addition to the fundamental component at $f=10$ MHz, both the first subharmonic and the second harmonic components are clearly seen at $f/2=5$ MHz and $2f=20$ MHz. Thus, the amplification voltage of 150 V_{p-p} seems to be above the harmonic generation threshold. It can be also noticed that the subharmonic intensity becomes almost the same as the second harmonic intensity after calibration of the

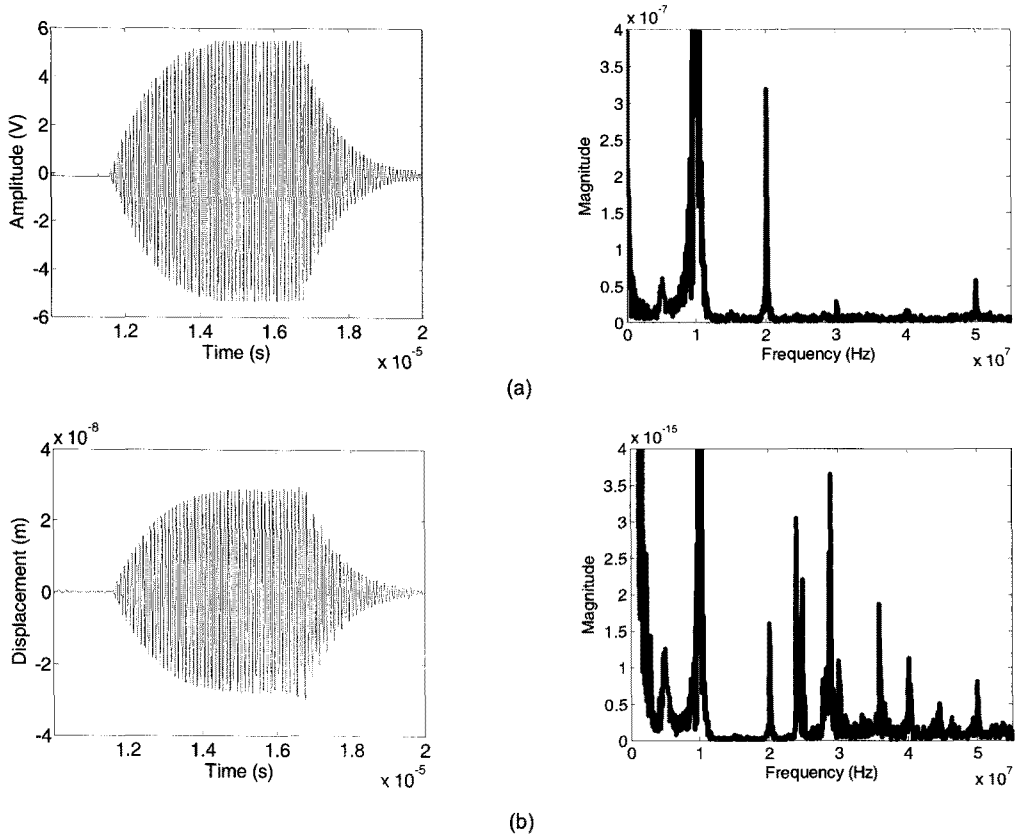


Fig. 6 Harmonic generation measurement at position 2 with 0 dB input excitation: Received waveform and Fourier spectrum before calibration; Received waveform and Fourier spectrum after calibration

received signal. We focus on these two harmonic components for further discussion below for nonlinearity parameter variation along the crack surface.

As described previously, the nonlinearity parameters for the first subharmonic and the second superharmonic were defined as $\beta'_{1/2} = A_{1/2}/A_1^2$ and $\beta'_2 = A_2/A_1^2$, respectively. These values were obtained from the slope of the A_1^2 vs. $A_{1/2}$ and A_1^2 vs. A_2 plots, respectively. Figs. 7 and 8 show these plots before calibration. Similar plots were found after calibration. The slope of the curve at each position was obtained from the best linear fit to the corresponding curve.

The measured nonlinearity parameter for the subharmonic component ($\beta'_{1/2}$) and for the

second harmonic component (β'_2) are shown in Fig. 9 before and after calibration. Both parameters are seen to be very small near the crack end and then increase rapidly as the measuring point moves toward the crack opening direction. The results of the second harmonic nonlinearity (β'_2) are qualitatively consistent with the previous work by Lee and Jhang (2009) where, using the uncalibrated receiving transducer output signal, the ratio of the second harmonic to the square of the fundamental also decreased toward the crack end. This behavior can be expected because a certain part of the crack produced by the fatigue loading can be treated as a partially closed crack and they will act as interface harmonic generators of different level. If the crack is too

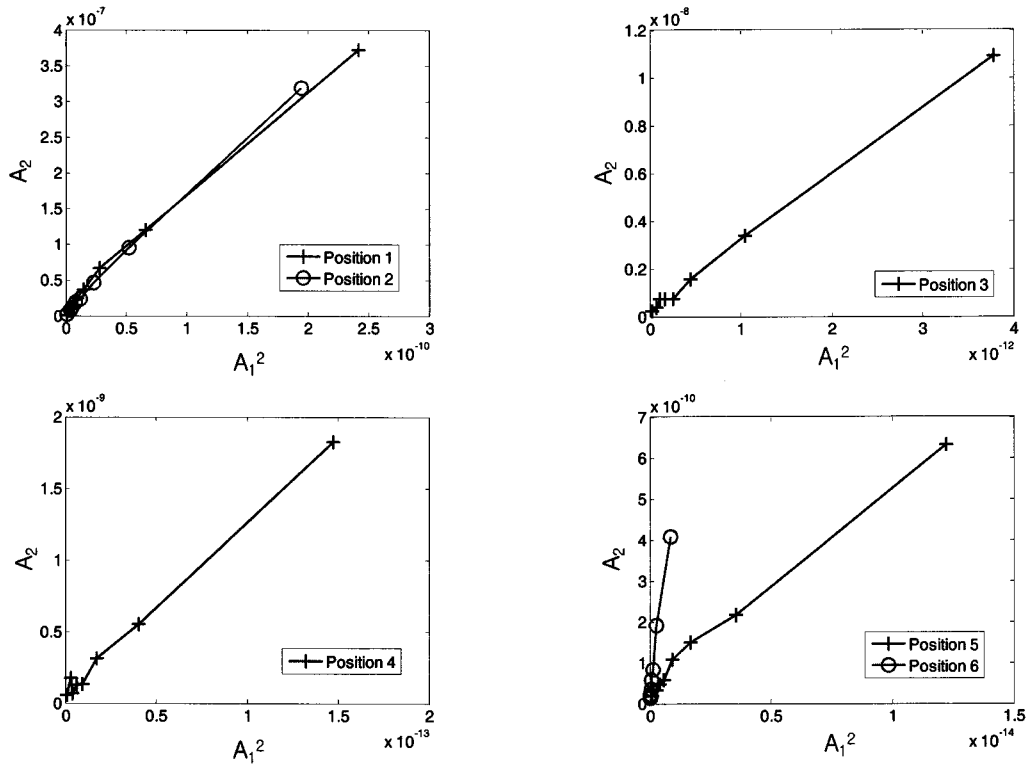


Fig. 7 A_1^2 vs. A_2 plot for the second superharmonic at six measurement positions before calibration

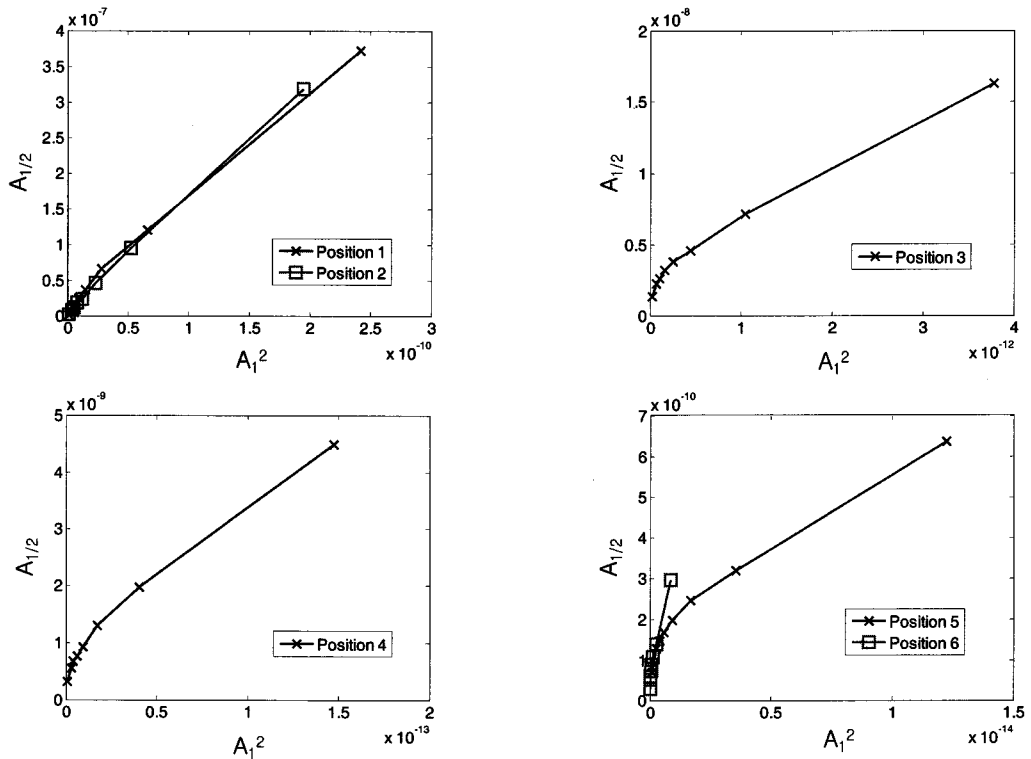


Fig. 8 A_1^2 vs. $A_{1/2}$ plot for the first subharmonic at six measurement positions before calibration

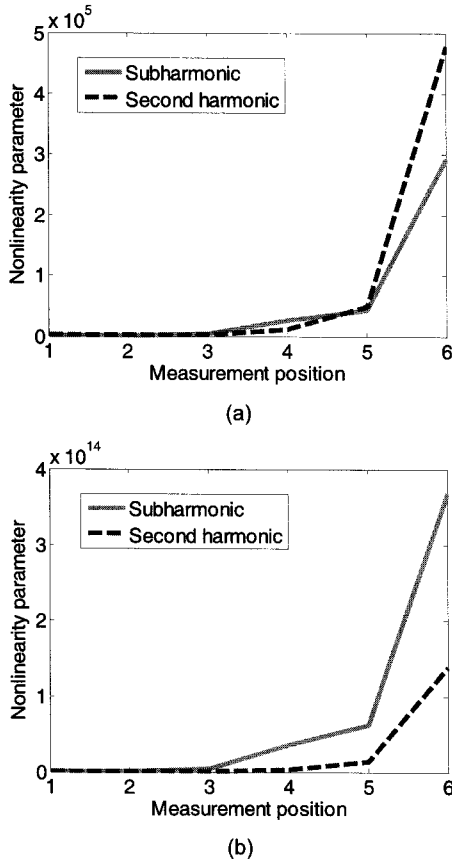


Fig. 9 Variation of nonlinearity parameter as a function of measurement position: (a) Before calibration; (b) After calibration

open to transmit the incident wave, most of the incoming wave will be reflected from the crack surface. The degree of harmonic generation will depend on the roughness of the surface and on the magnitude of the cohesive forces that arise from the small crack openings. This dependence will be further discussed in the model simulation below.

When the calibrated received signal was used in the nonlinearity parameter calculation, the subharmonic components generally provide higher nonlinearity parameters than those of the second harmonic components (Fig. 9(b)).

4. Model Prediction for Harmonic Generation

Sasaki et al. (2005) proposed a nonlinear

dynamic model for a partially closed crack when the wavelength is much longer than the crack size. They assumed that harmonics are generated by the clapping between the input and output crack planes. Their model was used for simulation of subharmonic generation at a surface-breaking crack under bending loads. In the model, the input crack plane vibrates with predetermined amplitude and frequency in the form of $a\sin\omega t$, while the output crack plane is represented by the mass m and the spring of stiffness k . When the input crack plane vibrates with a sufficiently large amplitude, this crack plane displaces the output crack plane by contact. Thus, the input crack plane exerts an interaction force on the other crack plane, depending on the crack opening displacement (COD). Under the harmonic excitation, the equation of the motion of the output crack plane is given by (Sasaki et al., 2005)

$$m\ddot{x} + \gamma\dot{x} + k(x - x_s) = f_0 \left[\kappa \left(\frac{\sigma}{x - a\sin\omega t} \right)^M - \left(\frac{\sigma}{x - a\sin\omega t} \right)^N \right] \quad (3)$$

where $x(t)$ is the position of the output crack plane, a is the input wave amplitude, ω is the input wave frequency, γ is the viscosity of vibration and x_s is the equilibrium position of the output crack plane without the interaction force. In eqn. (3) f_0 is the magnitude of force, M is the repulsive force index, N is the attractive force index, κ is the weight of repulsive force relative to attractive force and ω is the characteristic length of crack plane (e.g., interatomic distance, grain size or asperity height, etc.).

Fig. 10 shows calculated input and output waveforms and their frequency contents. Numerical values for various parameters were $M=9$, $N=3$, $\kappa=1$, $f_0=30\sigma$, $\omega=1$, $a=15\sigma$, $m=1$, $k=0.2$, and $\gamma=0.5$. The output waveforms are plotted with $x_s=11\sigma$. In the plot of input waveform, the time scale was adjusted to have a

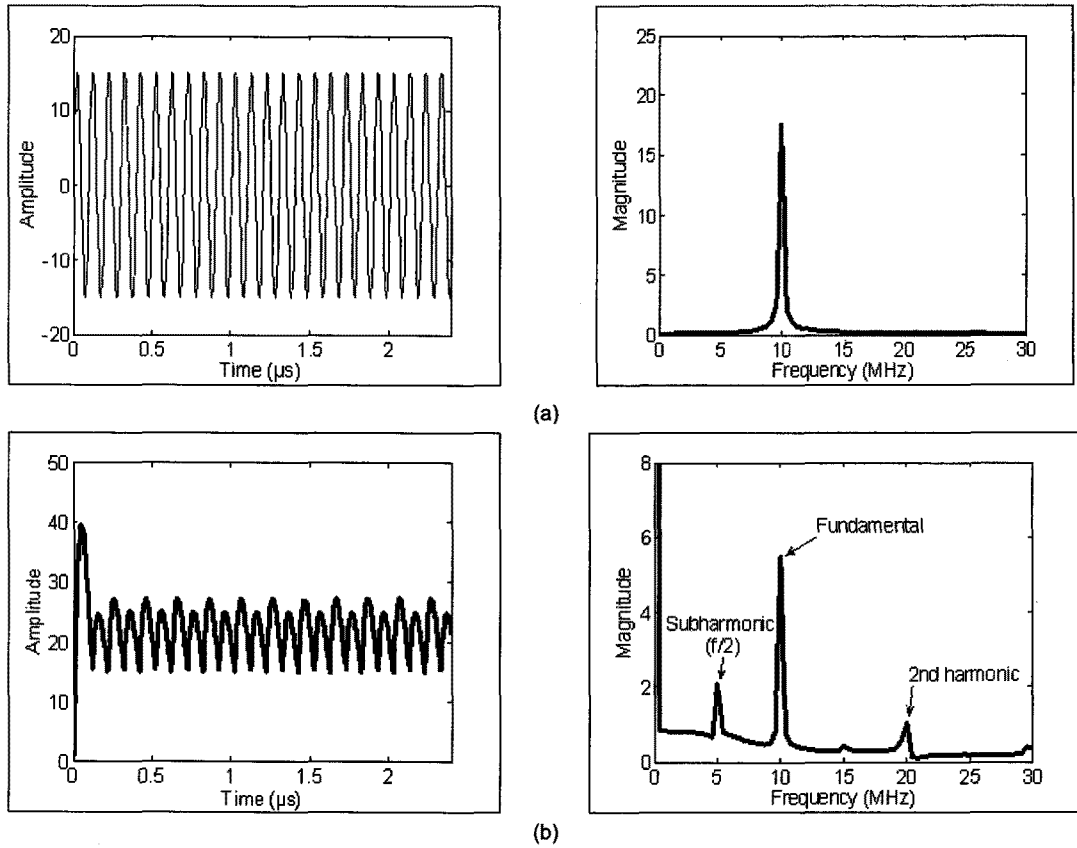


Fig. 10 Simulation results for harmonic generation at a crack interface: (a) Input waveform and Power spectrum; (b) Output waveform and power spectrum

period corresponding to the fundamental frequency of $f=10$ MHz. The amplitude scale was normalized by σ .

In the power spectrum of output signal (Fig. 10(b)), frequency components of the first subharmonic wave ($f/2=5$ MHz) and ultra-subharmonic wave ($3f/2=15$ MHz) are observed. Higher harmonic components of $2f=20$, $3f=30$ MHz are also clearly seen. The intensity of the first subharmonic wave at $f/2$ is found to be slightly larger than that of the second harmonic wave at $2f$. Thus, except for the relatively low power spectrum (or amplitude) at fundamental frequency f , this nonlinear dynamic model for cracked interfaces can be used to qualitatively explain the harmonic generation behavior observed at the real fatigue crack of CT specimen (Fig. 8).

5. Conclusions

Harmonic generation at a real cracked interface of a compact tension(CT) specimen was studied in this work. Two dominant harmonic components were experimentally identified as the first subharmonic at frequency $f/2$ and the second harmonic at $2f$ with the interrogation signal of frequency of f . Nonlinear parameters of these two harmonics were defined and measured at several positions on the specimen, and showed a variation that is consistent with a gradually closing crack toward the crack end. In the present study, the nonlinearity parameter of $f/2$ generally had a higher value after calibration of output signals. We are going to further study the optimal generation of the subharmonics for more reliable

detection and characterization of crack-like flaws.

Acknowledgement

This work was supported by the Nuclear R&D program through the Korea Science and Engineering Foundation funded by the Ministry of Education, Science and Technology.

References

- [1] K.-Y. Jhang, "Nonlinear ultrasonic techniques for nondestructive assessment of micro damage in material: A review," *International Journal of Precision Engineering and Manufacturing*, Vol. 10, pp. 123-135 (2009)
- [2] J. M. Richardson, "Harmonic generation at an unbonded interface - I. Planar interface between semi-infinite elastic media," *International Journal of Engineering Science*, Vol. 17, pp. 73-85 (1979)
- [3] J. D. Achenbach and A. N. Norris, "Loss of specular reflection due to nonlinear crack-face interaction," *Journal of Nondestructive Evaluation*, Vol. 3, pp. 229-239 (1982)
- [4] S. Hirose and J. D. Achenbach, "Higher harmonics in the far-field due to dynamic crack-face contacting," *Journal of the Acoustical Society of America*, Vol. 93, pp. 142-147 (1993)
- [5] O. Buck, W. L. Morris and J. M. Richardson, "Acoustic harmonic generation at unbonded interfaces and fatigue cracks," *Applied Physics Letters*, Vol. 33, pp. 371-373 (1978)
- [6] J. H. Cantrell and W. T. Yost, "Nonlinear ultrasonic characterization of fatigue microstructures," *International Journal of Fatigue*, Vol. 23, pp. 487-490 (2001)
- [7] D. J. Barnard, G. E. Dace and O. Buck, "Acoustic harmonic generation due to thermal embrittlement of Inconel 718," *Journal of Nondestructive Evaluation*, Vol. 16, pp. 67-75 (1997)
- [8] K. Y. Jhang, "Applications of nonlinear ultrasonics to the NDE of material degradation," *IEEE-UFFC*, Vol. 47, pp. 540-548 (2000)
- [9] H. Jeong, S. H. Nahm, K. Y. Jhang and Y. H. Nam, "A nondestructive method for estimation of the fracture toughness of CrMoV rotor steels based on ultrasonic nonlinearity," *Ultrasonics*, Vol. 41, pp. 543-549 (2003)
- [10] W. L. Morris, O. Buck and R. V. Inman, "Acoustic harmonic generation due to fatigue damage in high-strength aluminum," *Journal of Applied Physics*, Vol. 50, pp. 6737-6741 (1979)
- [11] T. H. Lee and K.-Y. Jhang, "Experimental investigation of nonlinear acoustic effect at crack," *NDT&E International*, Vol. 42, pp. 757-764 (2009)
- [12] A. Wegner, A. Koka, K. Janser, U. Netzelmann, S. Hirsekorn and W. Arnold, "Assessment of the adhesion quality of fusion-welded silicon wafers with nonlinear ultrasound," *Ultrasonics*, Vol. 38, pp. 316-321 (2000)
- [13] M. Rothenfusser, M. Mayr and J. Baumann, "Acoustic nonlinearities in adhesive joints," *Ultrasonics*, Vol. 38, pp. 322-326 (2000)
- [14] K. Yamanaka, T. Mihara and T. Tsuji, "Evaluation of closed cracks by model analysis of subharmonic ultrasound," *Japanese Journal of Applied Physics*, Vol. 43, pp. 3082-3087 (2004)
- [15] R. Sasaki, T. Ogata, Y. Ohara, T. Mihara and K. Yamanaka, "Simulation and analysis of subharmonics and tail effect for ultrasonic nondestructive evaluation of closed cracks," *Japanese Journal of*

- Applied Physics*, Vol. 44, pp. 4389-4393 (2005)
- [16] F. Semperlotti, K. W. Wang and E. C. Smith, "Localization of a breathing crack using nonlinear subharmonic response signals," *Applied Physics Letters*, Vol. 95, pp. 254101-1~3 (2009)
- [17] P. M. Shankar, P. D. Krishna and V. L. Newhouse, "Subharmonic backscattering from ultrasound contrast agents," *Journal of the Acoustical Society of America*, Vol. 106, pp. 2104-2110 (1999)
- [18] A. Moussatov, V. Gusev and B. Castagne'de, "Self-Induced hysteresis for nonlinear acoustic waves in cracked material," *Physical Review Letters*, Vol. 90, pp. 124301-1~4 (2003)
- [19] G. E. Dace, R. B. Thompson and O. Buck, "Measurement of the acoustic harmonic generation for material characterization using contact transducers," *Review of Progress in Quantitative Nondestructive Evaluation*, Vol. 11B, pp. 2069-2076 (1992)